Enhancement of Pool Boiling Heat Transfer Using Aligned Silicon Nanowire Arrays

Dong Il Shim,[†] Geehong Choi,[†] Namkyu Lee,[†] Taehwan Kim,[†] Beom Seok Kim,[‡] and Hyung Hee Cho*,[†]

[†]Department of Mechanical Engineering, Yonsei University, 50 Yonsei-ro, Seodaemun-gu, Seoul 120-749, Korea
[‡]IFW Dresden, P.O. Box 270116, 01171 Dresden, Germany

Ⓢ Supporting Information

ABSTRACT: Enhancing the critical heat flux (CHF), which is the capacity of heat dissipation, is important to secure high stability in two-phase cooling systems. Coolant supply to a dry hot spot is a major mechanism to prevent surface burn-out for enhancing the CHF. Here, we demonstrate a more ready supply of coolant using aligned silicon nanowires (A-SiNWs), with a high aspect ratio (>10) compared to that of conventional random silicon nanowires (R-SiNWs), which have a disordered arrangement, for additional CHF improvement. We propose the volumetric wicking rate, which

represents the coolant supply properties by considering both the liquid supply velocity and the amount of coolant (i.e., wicking coefficient and wetted volume, respectively). Through experimental approaches, we confirm that the CHF is enhanced as the volumetric wicking rate is increased. In good agreement with the fabrication hypothesis, A-SiNWs demonstrate higher coolant supply abilities than those of R-SiNWs. The longest (7 μm) A-SiNWs have the highest volumetric wicking rate (25.11 × 10^{-3} mm^3/s) and increase the CHF to 245.6 W/cm^2, which is the highest value obtained using nanowires among reported data (178 and 26% enhanced vs unmodulated plain surface and R-SiNWs, respectively). These well-aligned SiNWs can increase the CHF significantly with efficient coolant supply, and it can ensure high stability in extremely high thermal load systems. Moreover, our study provides nanoscale interfacial design strategies for further improvement of heat dissipation.

KEYWORDS: Surface modification, aligned nanowires, heat transfer enhancement, interfacial wicking, boiling heat transfer
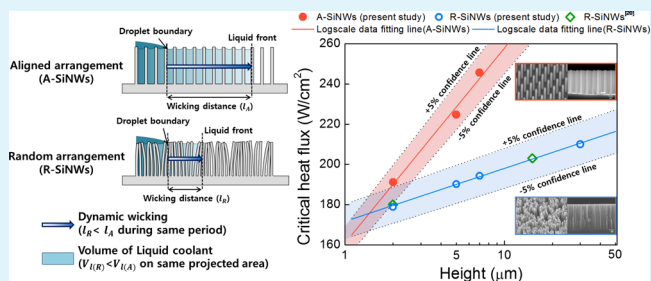
1. INTRODUCTION

Improving the heat-transfer performance should be considered for guaranteeing the efficiency and stability of energy systems. Boiling heat transfer is a powerful cooling mechanism accompanying the phase change phenomena. It has been used for cooling of high-thermal-load systems, such as power plants and integrated electrical devices.[1,2] Especially, the critical heat flux (CHF), which is the heat-transfer capacity (i.e., limitation of heat dissipation), is a key factor for maintaining a thermally stable system. The CHF is defined as the heat flux required to remove the thermal energy before film boiling. During film boiling, the vapors start to cover the overall heating area and cause surface failure because of a sharp thermal load from the low thermal conductivity of the vapor. For this reason, the CHF is closely related to the surface stability and the ability of high heat flux dissipation.[3−6] Therefore, achievement of high CHF ensures the performance and safety of thermal systems.

The recent research obviously has demonstrated that liquid supply to a dry area is the main mechanism for preventing vapor coverage to accomplish a higher CHF.[7−10] Surface interfacial manipulation methods have been applied for enhancing the boiling heat transfer characteristics. In particular, microscale and nanoscale structural manipulations have been

used on boiling surfaces to not only augment the surface area but also improve the liquid supplying properties, which are surface wettability and wicking.[11−15] Specifically, nanoscale structural manipulations, such as nanowire arrays, have enhanced the boiling performance significantly.[16−18] Silicon nanowire (SiNW) and copper nanowire (CuNW) arrays have been used for boiling heat transfer and achieved 100% higher CHF than that from a plain surface.[17,19] The wettability of the surface has been made superhydrophilic via fabrication of nanowires, and the capillary liquid propagation effect through the nanostructures had a positive aspect in coolant supply for enhancing the CHF. Moreover, many studies have been conducted using nanowires of various heights to enhance the boiling performance and to confirm CHF enhancement mechanisms.[16,20−22] Wettability has been improved with the increasing height of nanowires, and nucleation characteristics are favorable for heat transfer enhancement by increasing the defects or microscale cavities. The results commonly show effective improvement of CHF compared to that of plain
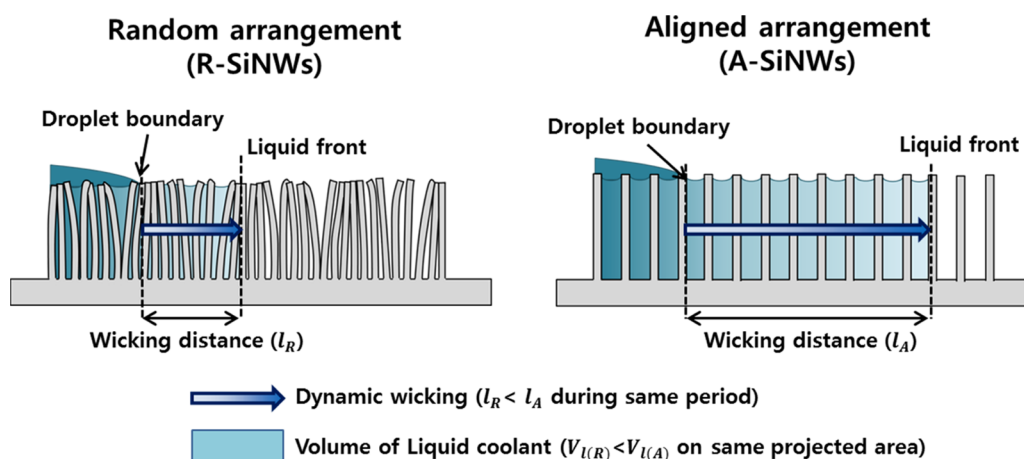
Figure 1. Strategy for enhancing the CHF of boiling heat transfer using A-SiNWs; R-SiNWs have a disordered arrangement and dense distribution. On A-SiNWs, dynamic wicking abilities are enhanced by reducing the fluidic resistance with a wicking-favorable arrangement. Moreover, the volume of the liquid coolant on A-SiNWs is larger than that on R-SiNWs on the same projected area.

surface; however, the CHF enhancement rate have a saturated trend ($\sim$220 W/cm^2). These conventional "random silicon nanowires (R-SiNWs)" have the limitation of being unable to enhance the CHF because nanoscale structures get entangled with each other and make bundlelike shapes. These complex distributions of nanostructures and high solid fractions increase the fluidic resistance and block the liquid spreading to dry regions.

For additional enhancement of CHF on NWs, improving the liquid supply to dry regions is important to prevent vapor film coverage on heating surfaces. Wicking, which occurs by capillary pressure by interfacial structures, is one of the key mechanisms of liquid propagation on a surface. For this reason, a wicking-favorable structured surface can improve the CHF. Recent research studies obviously have demonstrated that the wicking or liquid spreading phenomena on structured surfaces directly contribute to CHF enhancements by increasing the liquid supply to dry spots and additional heat dissipation from the wicking coolant. Superhydrophillic nanostructures, which were fabricated by an anodic oxidation process, biological templates, and nanopillars have been applied for boiling heat transfer for investigating the relation between wicking and boiling performance.[8−10] In these studies, the authors measured the amount of absorbed liquid volume by droplet images or measured the wicking coefficient by high-speed images for evaluating the coolant supply abilities on modified surfaces. They suggested similar wicking models, whereby the additional CHF enhancement occurred due to the wicking phenomena. Although previous studies, which have used surface modification, investigated the relation of wicking phenomena and CHF on boiling heat transfer, the rate of CHF enhancement has been demonstrated an obvious saturation tendency. There is no notable improvement in the boiling performance on nanostructured surfaces, such as conventional random nanowires and wicking-enhanced structured surfaces. Moreover, previous studies have relied on the wicking measurement of randomly fabricated surfaces. Therefore, it is difficult to analyze the geometric effect on wicking and its impact on boiling heat transfer. Here, we applied a strategic approach for the fabrication of nanowires to improve liquid supply and overcome the limitation of CHF on nanostructured surfaces.

Wicking is described by capillary pressure (P_{cap}) and viscous resistance (K). Capillary pressure generates a driving force for wicking, whereas viscous resistance interrupts liquid propagation. Then, the wicking distance (l) is defined as follows[23−25]

$$l = \sqrt{\frac{2P_{cap}}{K}t} = W\sqrt{t}$$

(1)

where W is the wicking coefficient, which represents the liquid propagation velocity. According to eq 1, high capillary pressure and low viscous resistance lead to a high wicking coefficient. There are three geometric parameters of A-SiNWs, which are diameter (d), pitch (p), and height (h). As d/p is increased, both capillary pressure and viscous resistance are increased. After the specific maximum values of the wicking properties are attained, the viscous resistance is increased rapidly compared with the capillary pressure and wicking abilities are decreased.[24,25] Thus, a wicking-favorable surface can be obtained by appropriate geometrical control. As reported by Xiao et al.,[25] the maximum wicking abilities on pillar arrays were observed for the dimensionless geometric parameter (d/p) from about 0.2 to 0.3 at the same height. However, on the R-SiNW surface, the nanostructures are arranged densely, for which d/p is more than 0.5, from scanning electron microscope (SEM) images.[17,26] Thus, the amount of fresh liquid supply on R-SiNWs is small because of both the low wicking coefficient from the high viscous resistance and the low wetted volume from the high solid fraction.

Our goal in this study is CHF enhancement by improving the liquid supply abilities using strategically aligned nanowire arrays. Figure 1 demonstrates the strategies for enhancing the CHF in this study. We fabricate "aligned silicon nanowires (A-SiNWs)" that stand independently and maintain a constant pitch and arrangement of nanostructures. A-SiNWs are fabricated to increase the liquid supply by two mechanisms for improving the CHF: First, A-SiNWs stand independently with a low solid fraction; thus, we expect that the wetted area would be expanded, thereby improving the capacity of the coolant for additional heat dissipation. Therefore, the liquid volume of A-SiNWs ($V_{l(A)}$) is larger than that of R-SiNWs ($V_{l(R)}$) on the same projected area. Additionally, different heights of R-SiNWs and A-SiNWs are fabricated to evaluate the effects of the wetted volume (i.e., the amount of fresh coolant). Second, we control the pitch-to-diameter ratio of nanowires for enhancing the wicking coefficient, which represents the velocity
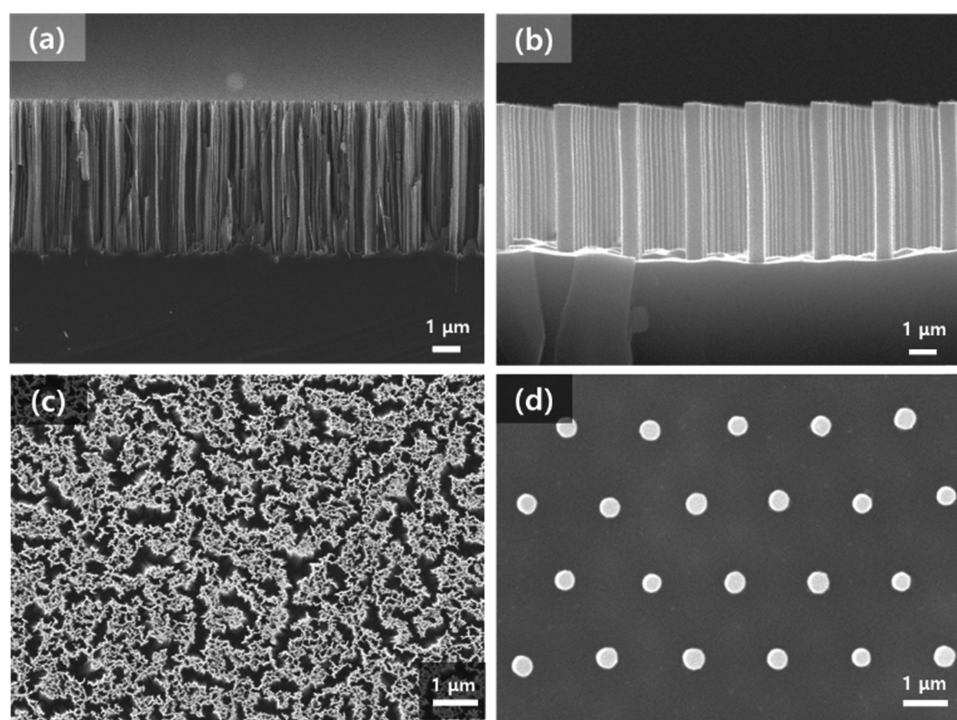
Figure 2. SEM images of 5 μm long R-SiNWs: a cross-sectional view of (a) R-SiNWs and (b) A-SiNWs; a top view of (c) R-SiNWs and (d) A-SiNWs. On R-SiNWs, nanostructures are attached with each other by Van der Waals forces and form a disordered arrangement. On the other hand, nanostructures are independent and maintain regular arrangement on A-SiNWs. In this study, various heights of SiNWs are used for boiling heat transfer, and fabrication results are shown in Figure S1.

of liquid propagation to dry regions. The aligned arrangement can reduce the fluidic resistance from independent and sparse arrays of structures. Thus, the wicking distance, which is defined as the length from the static droplet boundary to the dynamic spreading liquid front, is increased on A-SiNWs during the same period ($l_A > l_R$). To confirm the improvement of CHF on the strategically aligned arrangement, wicking and pool boiling experiments are conducted on A-SiNWs and R-SiNWs.

2. MATERIALS AND METHODS

2.1. Fabrication of R-SiNW and A-SiNW Surfaces on a Silicon Chip. SiNWs were fabricated on the backside of a silicon sensor chip, which can measure the wall temperature and input the power to the test sample simultaneously. For conventional R-SiNW fabrication, a metal-assisted chemical etching (MaCE) process was conducted.[11,27,28] The backside of the silicon sensor chip was cleaned with acetone for 10 min, with piranha solution (H_2O_2/H_2SO_4 = 1:3 by volume) for 40 min to remove organic materials, and with buffered oxide etchant (HF/H_2O = 1:5 by volume) for 5 min to remove any oxidation layer. After cleaning, the silicon sensor chip was inserted in a polytetrafluoro-ethylene etching module, which exposed only the center of the chip. Then, the etching module was immersed in a silver reducing solution (5 mM $AgNO_3$ and 4.8 M HF) for 1 min to reduce the silver ions on the silicon sensor chip. After rinsing the silicon sensor chip using deionized (DI) water, the etching module was immersed in the etchant solution (4.8 M HF and 0.1 M H_2O_2). The reduced silver ions act as the cathode, and H_2O_2 was reduced to H_2O. Also, silver ions generate electric holes that are injected on the silicon sensor chip.[27] Then, the silicon chip was oxidized and etched out with the HF solution.

We used a p-type silicon wafer substrate (boron-doped, (100) orientation, with a resistivity between 1 and 20 Ω cm); thus, silicon was etched down to form high-aspect-ratio nanowires. During the etching process, silver was the catalyst for etching down the silicon substrate. The height of the nanowire array could be controlled by the etching time. Thus, we fabricated 2, 5, 7, and 30 μm long R-SiNWs. The structures formed a disordered arrangement, and it was difficult to

control the accurate parameters of nanowires, such as diameter and pitch. For this reason, previous studies have reported the parameters of nanowires by morphological analyses, such as by SEM images.[17,20] In the same way, we estimated the diameter and pitch to be 100 and 200 nm, respectively. Figure 2a,c shows the cross-sectional and top views of 5 μm long R-SiNWs. The other fabrication results of R-SiNWs are shown in Figure S1.

For A-SiNWs fabrication, an additional nanosphere lens lithography process was carried out. After cleaning, the sensor chip was coated with a negative photoresist (PR) by spin-coating. A polystyrene monolayer was formed on the PR layer, and 500 nm diameter PR patterns were fabricated on the surface by nanosphere lens lithography and a PR strip. A gold thin film was deposited on the bare spaces, and silicon was etched by a MaCE process to fabricate nanowires. In the A-SiNW fabrication process, PR dots were the seeds of the nanowires and gold was the catalyst to etch the silicon substrate. The pitch of the nanowire was determined by the diameter of the nanospheres. Especially, d/p was controlled to 0.25, the wicking-favorable design for maximizing the liquid propagation velocity. We used 2 μm diameter spheres to form the monolayer; thus, the pitch of the nanowire array was 2 μm and the diameter of the nanowires was 500 nm. We confirmed that the nanowires stood independently and did not have random-sized microcavities by conglomeration of nanowires in SEM images. Figure 2b,d shows the cross-sectional and top views of 5 μm long A-SiNWs. The details of fabrication results are described in the Supporting Information.

2.2. Surface Characteristics (Morphology and Wetting Properties). The surface morphology of nanowires was observed by field emission-SEM (FE-SEM, JEOL 7800F). From the SEM images, we estimated the parameters of nanowires. Also, surface wetting properties, which are static wettability and dynamic wicking, were measured. The surface contact angle, which represents the static wettability, was measured by a contact angle meter (KSV, CAM-200). A DI water droplet (2.5 μL) was released on the surface, and cross-sectional images were taken by a 500 fps, high-speed camera. To observe the wicking phenomena and measure the wicking coefficient, DI water droplets were released on the SiNW surfaces. Immediately
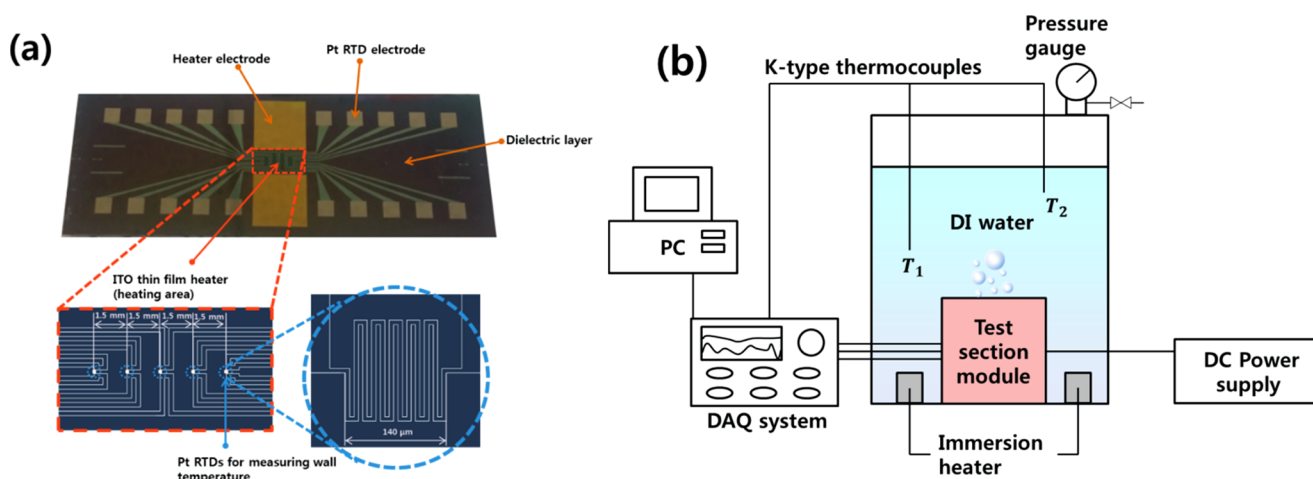
Figure 3. Experimental materials and setup: (a) a silicon sensor chip for supplying the heat load and sensing temperature; the sensor chip is composed of an ITO thin-film heater and Pt RTDs. Pt RTDs are fabricated in a serpentine shape for improving the accuracy and precision of the measurement. (b) Pool boiling experimental setup; the test section module is immersed in a stainless steel pool, and the heat load is generated by dc power supply. DI water is maintained at saturated temperature and atmospheric pressure.

after dropping the droplet on the surface, liquid propagation was observed and recorded by a 100 fps, high-speed camera (Dantec, Speedsense M310). Through analyzing high-speed images, the wicking distance was measured with the passage of time. Then, the wicking coefficient could be calculated from eq 1.

2.3. Pool Boiling Experiment. For data acquisition and heating the boiling surface, a silicon sensor chip was fabricated that could measure local temperatures and supply the heat flux, as shown in Figure 3a. The silicon sensor chip is composed of an indium tin oxide (ITO) thin-film heater and platinum resistance temperature detectors (Pt RTDs). The pool boiling experimental apparatus is shown in Figure 3b. We used DI water for the experimental working fluid. DI water was maintained at atmospheric pressure and saturated temperature by two immersion heaters and a proportional–integral–derivative controller. Two K-type thermocouples measured the temperature at different locations in the DI water. A power supply (KSC Korea Switching, 200 V-10 A, dc) supplied heat flux to a test section with stable values. Heater voltage drop and circuit current were measured from the ITO thin film and the shunt resistance, respectively. The resistances of the RTD sensors were measured with a data acquisition module and board (SCXI-1503, PCI-6259; National Instruments). To minimize the thermal loss, the main test section was made of polyether ether ketone (PEEK), which has a low thermal conductivity (k_{PEEK} = 0.25 W/(m K)). A silicon sensor chip was attached on a Macerite ceramic plate ($k_{macerite}$ = 1.6 W/(m K)) to minimize thermal heat conduction and prevent surface breakdown at the CHF. Degassing in the test chamber was carried out with immersion heaters for 1 h before the experiment. The electrical data and wall temperature from the RTD sensor were measured for more than 30 s after reaching steady-state conditions. The resistances from the RTD sensors were acquired at a high frequency, 1000 Hz. The data reduction process and uncertainty analysis are described in the Supporting Information.

3. RESULTS AND DISCUSSION

3.1. Enhanced CHF on SiNWs. The pool boiling experiment results are shown in Figure 4. The CHF on the silicon plain surface is 88.1 W/cm^2. The CHFs are increased by 102% (177.6 W/cm^2), 116% (190.1 W/cm^2), and 121% (194.3 W/cm^2) on R-SiNW surfaces of 2, 5, and 7 μm, respectively. Also, the CHFs are increased by 117% (191.1 W/cm^2), 154% (224.7 W/cm^2), and 178% (245.6 W/cm^2) on A-SiNW surfaces of 2, 5, and 7 μm, respectively. The CHFs are greatly enhanced on both R-SiNWs and A-SiNW surfaces compared to those on
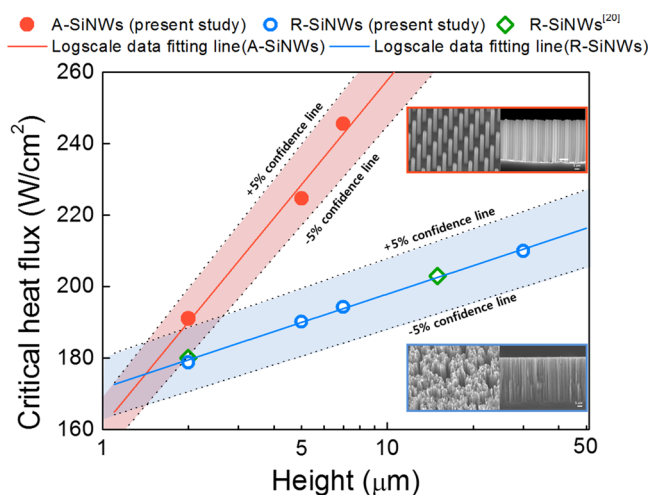

Figure 4. Pool boiling experimental results: the CHF is enhanced as the height of nanowires increases. The CHF on A-SiNWs is larger than that on R-SiNWs on the same height. In particular, the 7 μm long A-SiNWs enhance the CHF to 245 W/cm^2. The insets of the graph show the SEM images of A-SiNWs (red outline) and R-SiNWs (blue outline).

the plain surface. These results are consistent with the experimental results in a previous research, where the CHF has been enhanced using a hydrophilic nanowire surface in pool boiling heat transfer.[17,21] However, Figure 4 demonstrates obviously a different tendency on R-SiNWs and A-SiNWs. As the height of nanowires increases, the CHFs are enhanced drastically on A-SiNWs. In particular, on the longest A-SiNWs, the CHF was 245.6 W/cm^2, which is the highest reported value on nanowire surfaces. On the other hand, the CHF enhancement rate on R-SiNWs is decreased as the height of nanowires is increased. The CHFs on R-SiNWs reach a saturated value of about 200 W/cm^2 in longer cases.

Kandlikar[29,30] proposed a theoretical approach for CHF estimation on a horizontal heater, which reflects not only a classical hydrodynamic approach[31,32] but also surface wettability as follows

$$q''_{CHF\_Kandlikar} = h_{fg}\rho_g^{0.5}[\gamma g(\rho_1 - \rho_g)]^{0.25}[(1 + \cos\theta)/16]$$

$$[2/\pi + \pi/4(1 + \cos\theta)]^{0.5} \quad (2)$$

where h_{fg} is the latent heat of the fluid gas, ρ_g is the density of the gas, and ρ_1 is the density of the liquid. According to eq 2, a hydrophilic surface that has a low contact angle will have a high CHF because it is favorable for supplying the working fluid to the heating area and enhancing the CHF. Figure 5 shows the
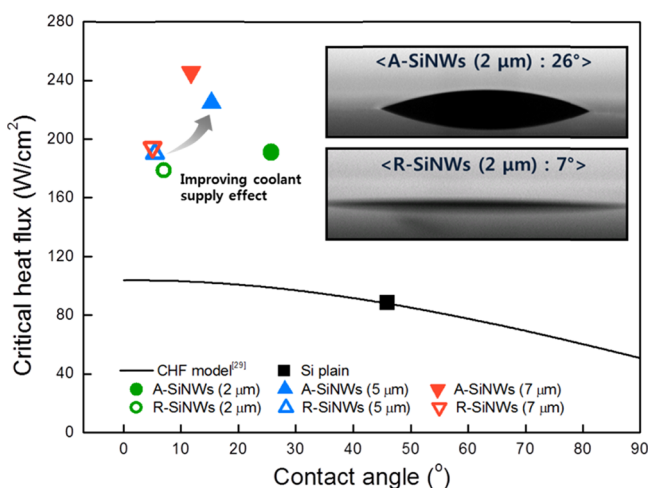
Figure 5. Comparison of the experimental data and CHF model, which considers surface wettability. Additional CHF enhancement occurred by improving the liquid coolant supply effect on SiNWs. Notably, A-SiNWs improve the CHF effectively despite larger contact angles (i.e., weaker superhydrophilicity) than those in R-SiNWs. The insets demonstrate the surface contact angles on 2 μm long A-SiNWs and R-SiNWs.

CHF results of the present experiments and CHF predictions by a Kandlikar's theoretical approach. The experimental result is consistent with the CHF model on the silicon plain surface. On the other hand, the experimental CHFs are much higher on both R-SiNWs and A-SiNW surfaces than those on the CHF model. This additional improvement of boiling performance has already been described by the liquid spreading or wicking phenomena on the structured surface.[8–10] Wicking can occur when the apparent contact angle is smaller than the critical contact angle (θ_c), which is defined as follows

$$\theta_c = \cos^{-1}[(1 - \varphi)/(r - \varphi)] \quad (3)$$

where φ is a solid fraction of nanowires and r is the roughness factor, which is the ratio of the actual area to the projected area. On the R-SiNWs, the arrangement is assumed to be a rectangular array; thus, $\varphi \equiv \pi d^2/4p^2$ and $r \equiv 1 + \pi dh/p^2$. On the other hand, on the A-SiNWs, the arrangement is a triangular array; thus, $\varphi \equiv \pi d^2/4p^2 \sin 60$ and $r \equiv 1 + \pi dh/p^2 \sin 60$. In particular, the solid fractions are 0.20 and 0.06 by geometric parameters of R-SiNWs and A-SiNWs, respectively.

It is successfully demonstrated that the wetted volume is enhanced on A-SiNWs by a smaller solid fraction. All cases in this study have a smaller apparent contact angle ($\theta_{Si} = 46°$) than the critical contact angle for wicking criteria (Table 1). Therefore, it is reasonable that the CHF is higher than that in theoretical model, which contains only the static wettability of the surface through an improving the coolant supply effect.

In these experimental results, there are two remarkable points. First, at the same height of nanowires, the CHF is larger on the A-SiNW surface than on the R-SiNW surface. On the A-SiNW surface, the CHF was enhanced by 7, 18, and 26%, compared to that on the R-SiNW surfaces of 2, 5, and 7 μm, respectively. In particular, although A-SiNWs have less hydrophilic characteristics (i.e., larger contact angles) than those of R-SiNWs, they have a higher value of CHF than that on the R-SiNW surface, which has the same height. These results obviously demonstrate that the liquid supply abilities are the dominant mechanisms for enhancing the CHF in a hydrophilic region. Second, the CHF was enhanced as the height of the nanowires increased. According to the experimental results, a longer height of the A-SiNW surface can remove a higher thermal load than that from a shorter height of the A-SiNW surface. These results demonstrate that the structured array morphology and the height of the nanowires are key factors for enhancing the CHF because of the improvement of liquid supplying mechanisms.

3.2. Evaluation of Wicking Properties of SiNWs. For analyzing the pool boiling experimental results that A-SiNWs have larger CHFs despite poor static wettability than those of R-SiNWs, wicking coefficients are investigated. As shown in Figure 6a, the wicking distance is defined as the distance from the static droplet boundary to the dynamic wicking liquid front. The details of the wicking image on each SiNW are demonstrated in Figure S2. Representatively, Figure 6b,c shows the wicking images of 7 μm long R-SiNWs and A-SiNWs at 4 s after droplet releasing. The images show an obvious tendency whereby A-SiNW surfaces have a larger wicking distance than that on the R-SiNW surfaces during the same time period. The analysis of the high-speed images taken to measure the wicking distance and the calculated wicking coefficient are shown in Table 1 and Figure 6d. The wicking coefficients are 0.31, 0.40, and 0.43 mm/s$^{0.5}$ on R-SiNWs of 2, 5, and 7 μm and 0.50, 1.70, and 1.95 mm/s$^{0.5}$ on A-SiNWs of 2, 5, and 7 μm, respectively. These results are in good agreement with the fabrication hypothesis that the aligned arrangement that has d/p of 0.25 can reduce the viscous resistance effectively and promote the liquid propagation velocity compared to those in the random arrangement. As a result, the wicking coefficient is precipitously raised on A-SiNW surfaces compared to that on R-SiNW surfaces. In addition, as the height of the nanowires increases, the capillary pressure increases, enhancing the liquid propagation. Thus, the wicking coefficients increase as the height of the nanowires is increased.

Table 1. Geometric Variables and Wicking Properties of SiNWs

|	R-SiNWs ($\varphi = 0.20$)			A-SiNWs ($\varphi = 0.06$)		
height (μm)	2	5	7	2	5	7
θ_c (degree)	87	89	89	59	73	77
W (mm/$\sqrt{s}$)	0.31	0.40	0.43	0.5	1.7	1.95
$W^2(1 - \varphi)h$ ($\times 10^{-3}$ mm^3/s)	0.18	0.73	1.18	0.47	13.63	25.11
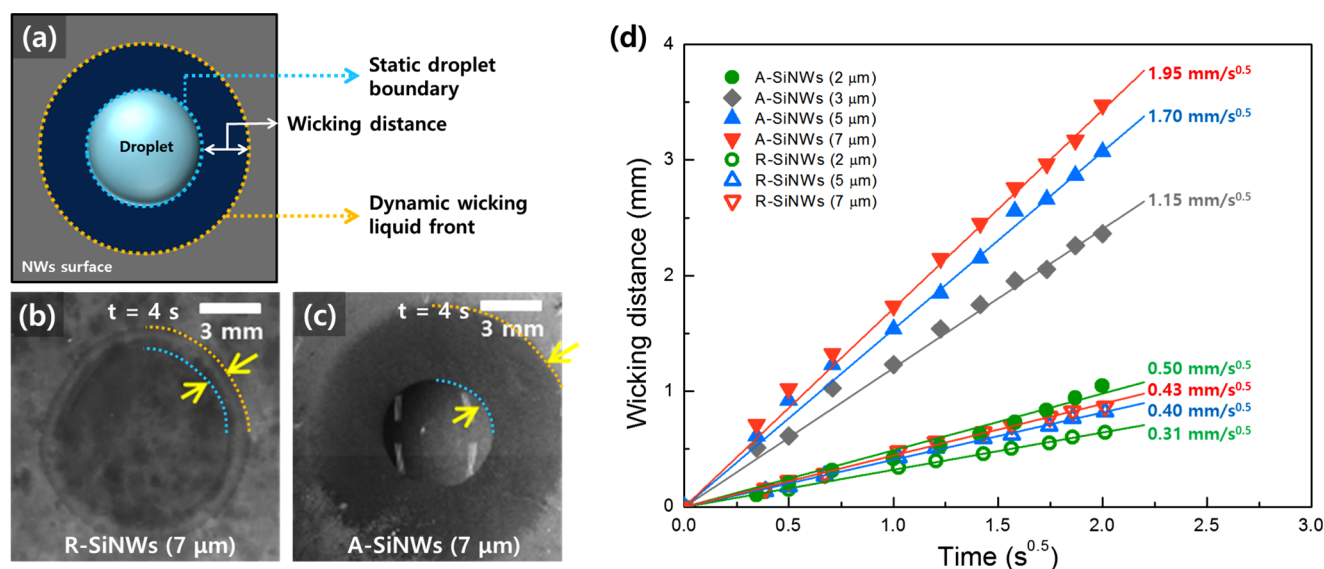
Figure 6. Wicking phenomena on SiNWs. (a) Schematic diagram of a droplet on SiNWs and the wicking distance. The blue dotted line represents a static droplet boundary and the yellow dotted line represents a dynamic wicking liquid front; high-speed images at 4 s after droplet releasing on (b) R-SiNWs (7 μm) and (c) A-SiNWs (7 μm); (d) wicking distance vs square root of time and wicking coefficient of R-SiNWs and A-SiNWs. The details of wicking experiment results on each SiNW are demonstrated in Figure S2.

3.3. Enhanced CHF by Improvement of Coolant Supply Using A-SiNWs.

Local hot spots occur during boiling heat transfer at a high heat flux. Both the wicking ability and wetted volume are the key factors in liquid supply characteristics because they have a strong connection with the speed of liquid propagation and the amount of additional heat dissipation capacity by evaporation, respectively. Therefore, A-SiNWs, which have high liquid supply ability, effectively prevent the formation of vapor films on the heated surface. Developing both the wicking rate and the wetted volume is a strategy for enhancing the CHF by improved coolant supply. Now, we propose that the volumetric wicking rate, $W^2(1 - \varphi)h$, is a unified factor for considering the wicking rate and wetted volume. Table 1 presents the wicking coefficients and volumetric wicking rates of each SiNW surface. The volumetric wicking rates are 0.18×10^{-3}, 0.73×10^{-3}, and 1.18×10^{-3} mm^3/s on R-SiNW surfaces of 2, 5, and 7 μm, and 0.47×10^{-3}, 13.63×10^{-3}, and 25.11×10^{-3} mm^3/s on A-SiNW surfaces of 2, 5, and 7 μm, respectively. On the same height of nanowire surfaces, the volumetric wicking rate of A-SiNW surfaces is increased by the enhanced wicking coefficient. In addition, as the height of the nanowires is increased, the volumetric wicking rate is enhanced because of the higher wetted volume. The volumetric wicking rate is improved on the A-SiNW surfaces with an aligned distribution and a long height. Figure 7 demonstrates that the CHF is enhanced by the coolant supply as the volumetric wicking rate is increased. The experimental results distinctly show the proportional relation with the volumetric wicking rate, that is, the coolant supply abilities. The pool boiling experimental results are consistent with the hypothesis that the liquid supply by the wicking phenomena can enhance additional heat dissipation, with extra improvement of CHF achieved on the aligned structured surfaces. The additional heat dissipation (q''_{add}) from the wicking phenomena can be expressed as a proportional relation as follows[10,33]

$$q''_{add} \propto W^2(1 - \varphi)h \qquad (4)$$
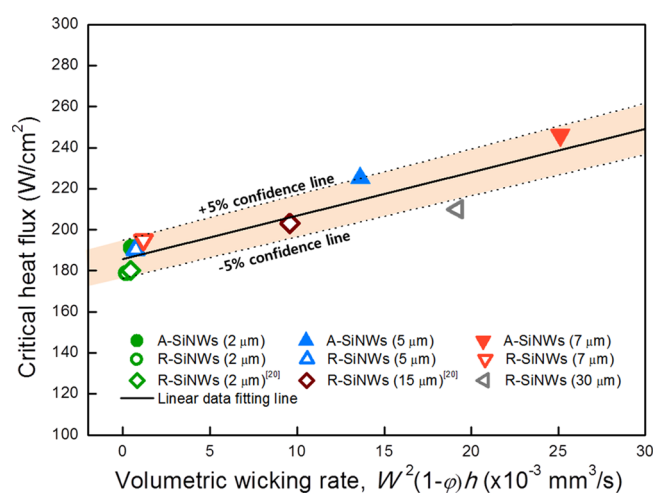
Figure 7. CHF vs volumetric wicking rate on A-SiNWs and R-SiNWs: the experimental results distinctly show the proportional relation with the volumetric wicking rate, that is, the coolant supply abilities. The volumetric wicking rate is enhanced by control of nanowire arrangement because of the relatively high wicking coefficient and low solid fraction.

A high volumetric wicking rate can remove the thermal energy rapidly and delay the formation of vapor film on a heating surface. Although the present A-SiNWs have a relatively short height than that of other R-SiNWs, it can achieve a higher CHF. Notably, A-SiNWs overcome the limitation of CHF on the nanowire surface by enhanced additional coolant supply using an artificially controlled arrangement.

4. CONCLUSIONS

In this study, enhanced CHF was accomplished by improving the coolant supply using strategically controlled A-SiNWs. We fabricated SiNWs strategically to enhance the coolant supply considering both the wicking coefficient and the wetted volume by fabrication of A-SiNWs, which stand independently and secure volume for refreshing with the coolant. Especially, a

wicking-favorable arrangement ($d/p \sim 0.25$) was chosen for improving the liquid supply velocity. Pool boiling experiments were conducted on a silicon plain surface and for various heights of R-SiNWs and A-SiNW to verify the hypothesis for enhanced CHF. To evaluate the coolant supply abilities, we propose the volumetric wicking rate, $W^2(1 - \varphi)h$, considering both the wicking coefficient (i.e., the liquid supply velocity) and the wetted volume. To measure the volumetric wicking rate, we evaluated the wicking coefficient on each SiNW and calculated the wetted volume on the basis of the geometric variables. The experimental results demonstrated that the CHF was enhanced with high volumetric wicking rate surfaces because of a positive effect on the liquid supply to the dry region for delaying vapor merging and removal of additional thermal energy. In particular, the longest A-SiNW (7 μm) surface had the largest value for the volumetric wicking rate (25.11×10^{-3} mm^3/s) and increased the CHF by 178% (245 W/cm^2) compared to that on a silicon plain surface. This result was also the highest value among the other reported data using nanowire surfaces. In conclusion, we confirmed a possibility of further CHF enhancement on structured surfaces using liquid supply improvement. The pool boiling results were in good agreement with the design hypothesis that high coolant supply properties on surfaces can enhance the CHF via additional thermal energy removal from the heating area efficiently. High coolant supply properties, represented by a high wicking coefficient and wetted volume, can be achieved via the strategically aligned arrangement. We expect that further CHF enhancement will be achieved by controlling the parameters of A-SiNWs, such as the diameter, pitch, and height, in future studies. Moreover, this newly structured fabrication strategy using nanowires to enhance the CHF can ensure the stability of extremely high thermal energy systems and effective thermal management.

ASSOCIATED CONTENT

Ⓢ Supporting Information

The Supporting Information is available free of charge on the ACS Publications website at DOI: 10.1021/acsami.7b01929.

> Details of experimental materials and methods, FE-SEM images, and wicking coefficients of SiNWs (PDF)

AUTHOR INFORMATION

Corresponding Author

*E-mail: hhcho@yonsei.ac.kr. Tel: +82 2 2123 2828. Fax: +82 2 312 2159.

ORCID ⓘ

Hyung Hee Cho: 0000-0001-5309-3798

Notes

The authors declare no competing financial interest.

ACKNOWLEDGMENTS

REFERENCES

(1) Fang, X.; Chen, Y.; Zhang, H.; Chen, W.; Dong, A.; Wang, R. Heat Transfer and Critical Heat Flux of Nanofluid Boiling: A Comprehensive Review. *Renewable Sustainable Energy Rev.* **2016**, *62*, 924−940.

(2) Li, D.; Wu, G. S.; Wang, W.; Wang, Y. D.; Liu, D.; Zhang, D. C.; Chen, Y. F.; Peterson, G. P.; Yang, R. Enhancing Flow Boiling Heat Transfer in Microchannels for Thermal Management with Monolithically-Integrated Silicon Nanowires. *Nano Lett.* **2012**, *12*, 3385−3390.

(3) Dhir, V. Boiling Heat Transfer. *Annu. Rev. Fluid Mech.* **1998**, *30*, 365−401.

(4) Ebadian, M. A.; Lin, C. X. A Review of High-Heat-Flux Heat Removal Technologies. *J. Heat Transfer* **2011**, *133*, 110801.

(5) Kandlikar, S. G. *Heat Transfer Mechanisms during Flow Boiling in Microchannels*, Proceedings of the first International Conference on Micro/Minichannels; ASME, 2003.

(6) Dhillon, N. S.; Buongiorno, J.; Varanasi, K. K. Critical Heat Flux Maxima during Boiling Crisis on Textured Surfaces. *Nat. Commun.* **2015**, *6*, No. 8247.

(7) Hu, Y.; Zhang, S.; Li, X.; Wang, S. Heat Transfer Enhancement Mechanism of Pool Boiling with Self-Rewetting Fluid. *Int. J. Heat Mass Transfer* **2014**, *79*, 309−313.

(8) Rahman, M. M.; Ölçeroğlu, E.; McCarthy, M. Role of Wickability on the Critical Heat Flux of Structured Superhydrophilic Surfaces. *Langmuir* **2014**, *30*, 11225−11234.

(9) Ahn, H. S.; Jo, H. J.; Kang, S. H.; Kim, M. H. Effect of Liquid Spreading due to Nano/Microstructures on the Critical Heat Flux during Pool Boiling. *Appl. Phys. Lett.* **2011**, *98*, No. 071908.

(10) Kim, B. S.; Lee, H.; Shin, S.; Choi, G.; Cho, H. H. Interfacial Wicking Dynamics and its Impact on Critical Heat Flux of Boiling Heat Transfer. *Appl. Phys. Lett.* **2014**, *105*, No. 191601.

(11) McCarthy, M.; Gerasopoulos, K.; Maroo, S. C.; Hart, A. J. Materials, Fabrication, and Manufacturing of Micro/Nano-Structured Surfaces for Phase-Change Heat Transfer Enhancement. *Nanoscale Microscale Thermophys. Eng.* **2014**, *18*, 288−310.

(12) Kim, D. E.; Yu, D. I.; Jerng, D. W.; Kim, M. H.; Ahn, H. S. Review of Boiling Heat Transfer Enhancement on Micro/Nano-structured Surfaces. *Exp. Therm. Fluid Sci.* **2015**, *66*, 173−196.

(13) Chu, K.-H; Enright, R.; Wang, E. N. Structured Surfaces for Enhanced Pool Boiling Heat Transfer. *Appl. Phys. Lett.* **2012**, *100*, No. 241603.

(14) Dong, L.; Quan, X.; Cheng, P. An Experimental Investigation of Enhanced Pool Boiling Heat Transfer from Surfaces with Micro/Nano-Structures. *Int. J. Heat Mass Transfer* **2014**, *71*, 189−196.

(15) Jo, H. J.; Yu, D. I.; Noh, H.; Park, H. S.; Kim, M. H. Boiling on Spatially Controlled Heterogeneous Surfaces: Wettability Patterns on Microstructures. *Appl. Phys. Lett.* **2015**, *106*, No. 181602.

(16) Lu, Y.-W; Kandlikar, S. G. Nanoscale Surface Modification Techniques for Pool Boiling Enhancement—A Critical Review and Future Directions. *Heat Transfer Eng.* **2011**, *32*, 827−842.

(17) Chen, R.; Lu, M.-C.; Srinivasan, V.; Wang, Z.; Cho, H. H.; Majumdar, A. Nanowires for Enhanced Boiling Heat Transfer. *Nano Lett.* **2009**, *9*, 548−553.

(18) Shin, S.; Choi, G.; Kim, B. S.; Cho, H. H. Flow Boiling Heat Transfer on Nanowire-Coated Surfaces with Highly Wetting Liquid. *Energy* **2014**, *76*, 428−435.

(19) Im, Y.; Joshi, Y.; Dietz, C.; Lee, S. S. Enhanced Boiling of a Dielectric Liquid on Copper Nanowire Surfaces. *Int. J. Micro-Nano Scale Transp.* **2010**, *1*, 79−96.

(20) Kim, B. S.; Shin, S.; Lee, D.; Choi, G.; Lee, H.; Kim, K. M.; Cho, H. H. Stable and Uniform Heat Dissipation by Nucleate-Catalytic Nanowires for Boiling Heat Transfer. *Int. J. Heat Mass Transfer* **2014**, *70*, 23−32.

(21) Yao, Z.; Lu, Y. W.; Kandlikar, S. G. Effects of Nanowire Height on Pool Boiling Performance of Water on Silicon Chips. *Int. J. Therm. Sci.* **2011**, *50*, 2084−2090.

(22) Shi, B.; Wang, Y.-B; Chen, K. Pool Boiling Heat Transfer Enhancement with Copper Nanowire Arrays. *Appl. Therm. Eng.* **2015**, *75*, 115−121.

(23) Washburn, E. W. The Dynamics of Capillary Flow. *Phys. Rev.* **1921**, *17*, 273−283.

(24) Xiao, R.; Wang, E. N. Microscale Liquid Dynamics and the Effect on Macroscale Propagation in Pillar Arrays. *Langmuir* **2011**, *27*, 10360−10364.

(25) Xiao, R.; Enright, R.; Wang, E. N. Prediction and Optimization of Liquid Propagation in Micropillar Arrays. *Langmuir* **2010**, *26*, 15070−15075.

(26) Wang, H.; Jiang, W.; Yuan, L.; Wang, L.; Chen, H. Reductase-like Activity of Silicon Nanowires Arrays. *ACS Appl. Mater. Interfaces* **2013**, *5*, 1800−1805.

(27) Huang, Z.; Geyer, N.; Werner, P.; de Boor, J.; Gosele, U. Metal-Assisted Chemical Etching of Silicon: A Review. *Adv. Mater.* **2011**, *23*, 285−308.

(28) Smith, B. D.; Patil, J. J.; Ferralis, N.; Grossman, J. C. Catalyst Self-Assembly for Scalable Patterning of sub 10 nm Ultrahigh Aspect Ratio Nanopores in Silicon. *ACS Appl. Mater. Interfaces* **2016**, *8*, 8043−8049.

(29) Kandlikar, S. G. A Theoretical Model to Predict Pool Boiling CHF Incorporating Effects of Contact Angle and Orientation. *J. Heat Transfer* **2001**, *123*, 1071−1079.

(30) Kandlikar, S. G.. *Insight into Mechanisms and Review of Available Models for Critical Heat Flux (CHF) in Pool Boiling*, first International Conference on Heat Transfer, Fluid Dynamics and Thermodynamics, 2002.

(31) Zuber, N. Hydrodynamic Aspects of Boiling Heat Transfer. Ph.D. Thesis, California University, Los Angeles, 1959.

(32) Haramura, Y.; Katto, Y. A New Hydrodynamic Model of Critical Heat flux, Applicable Widely to both Pool and Forced Convection Boiling on Submerged Bodies in Saturated Liquids. *Int. J. Heat Mass Transfer* **1983**, *26*, 389−399.

(33) Kim, B. S.; Choi, G.; Shin, S.; Gemming, T.; Cho, H. H. Nano-Inspired Fluidic Interactivity for Boiling Heat Transfer: Impact and Criteria. *Sci. Rep.* **2016**, *6*, No. 34348.